Screening and the pinch point paradox in spin ice

Mikael Twengström
Department of Physics, Royal Institute of Technology, 106 91 Stockholm, Sweden

Patrik Henelius
Department of Physics, Royal Institute of Technology, 106 91 Stockholm, Sweden
and Faculty of Science and Engineering, Åbo Akademi University, 20500 Åbo, Finland

Steven T. Bramwell
London Centre for Nanotechnology and Department of Physics and Astronomy, University College London, 17-19 Gordon Street, London WC1H OAH, United Kingdom

(Received 5 June 2019; revised manuscript received 9 January 2020; accepted 20 February 2020; published 12 March 2020)

Spin ice may be considered to be a model system for the investigation of pinch point scattering. We present very-high-resolution numerical simulations and an analytical theory of the pinch point profiles of the near-neighbor and dipolar spin ice models and find these to be in excellent agreement with each other and with existing theory. Most importantly, the pinch points of the dipolar spin ice model are infinitely sharp, as a result of unscreened dipolar fields. These results are compared to polarized neutron scattering measurements of the pinch point profiles in $Ho_2Ti_2O_7$, considered to be an accurate realization of dipolar spin ice. In contrast to the numerical and analytical results, the experimental pinch point profiles are shown to be broadened in a manner that is quantitatively consistent with fully screened dipolar fields. This striking paradox is not easily resolved: Possible resolutions implicate quantum fluctuations or fundamental corrections to the theory of simulation or polarized neutron scattering. We further discuss our results in the context of spin ice's role as a model Coulomb fluid.

DOI: 10.1103/PhysRevResearch.2.013305

I. INTRODUCTION

The pinch point [Fig. 1(a)] is a type of singularity that occurs in the scattering cross section of diverse types of condensed matter. Important examples include dipolar systems, such as ferromagnets [1,2] and ice-rule systems, which include hydrogen bonded ferroelectrics [3–6], water ice [7,8], spin ice [9–14], ionic ice [15,16], artificial spin ice [17–19], quantum spin ice [20–22], and antiferromagnetic spin liquids [23–27]. In contrast to the Landau description, many of these systems enter a highly correlated low-temperature state without any symmetry breaking.

The pinch point is expected to be a principal characteristic of such states (in some, but not all, of the above examples, Pauling entropy [28–30] is another key characteristic). However, despite its widespread relevance, the pinch point concept has barely been tested. This is because, in both simulation and experiment, particularly high resolution is required, while in experiment, high intensity is also necessary. In addition, well-defined model systems are scarce. Spin ice [31,32], whose pinch points arise from the combined effects of dipolar and ice-rule correlations [33] is an exception, a nearly ideal model system that lends itself well to advanced experiment and numerical modeling (see Fig. 2).

Classical spin ices like $Ho_2Ti_2O_7$ and $Dy_2Ti_2O_7$ are described by the dipolar spin ice (DSI) model [34], with the spin Hamiltonian consisting of exchange and dipolar terms:

$$\mathcal{H} = \mathcal{H}_{\text{exchange}} + \mathcal{H}_{\text{dipolar}}. \tag{1}$$

This model (along with its extensions [35]) is consistent with some surprising properties, including residual (Pauling) entropy [29], emergent electromagnetism [36,37], fractionalization [37], and fragmentation [38,39]. A truncation of the dipole-dipole interaction to the near-neighbor interaction in Eq. (1) gives the simpler near-neighbor spin ice (NNSI) model [31,32], which is a valuable point of reference.

The spin ices further represent model Coulomb fluids [37,40–44] (of magnetic monopoles). Neutron scattering therefore affords a rare opportunity to experimentally image the field correlations and screening in the Coulomb fluid, which may shed light on topical questions raised by experiments on ionic liquids [45,46].

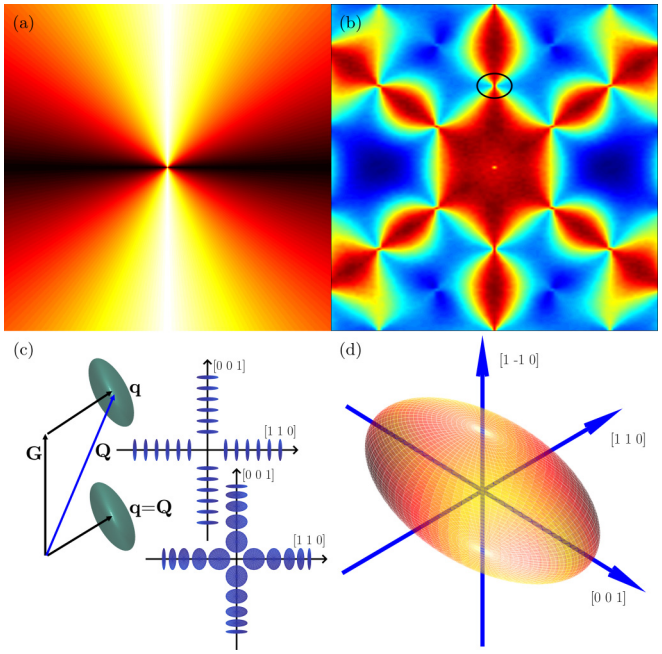

FIG. 1. (a) Pinch point. The function approaches a singularity in which its value at $q = 0$ (center of plot) depends on the orientation of any line passing through $q = 0$. (b) The (simulated) SF pattern of spin ice in the $1\bar{1}0$ scattering plane of reciprocal space; the pinch point at 002 is circled. (c) Shown on the left is the relation of the scattering vector $\mathbf{Q}$, reciprocal lattice vector $\mathbf{G}$, and $\mathbf{q} = \mathbf{Q} - \mathbf{G}$, illustrating the representative ellipsoid of the inverse of the structure factor tensor $S^{\alpha\beta}(\mathbf{q})$. The ellipsoid has different transverse projections on $\mathbf{Q}$ in the first zone (where $\mathbf{Q} = \mathbf{q}$) and higher zones (where $\mathbf{Q} = \mathbf{G} + \mathbf{q}$); it is these projections that are seen in neutron scattering. Shown on the right is how the ellipsoid varies with $\mathbf{q}$ in the case of sharp pinch points (upper, where the ellipsoid is eccentric at all finite q) and broadened pinch points (lower, where it becomes a sphere for small q). (d) Representation ellipsoid and principal axes of the inverse structure factor tensor along the line $hh2$ (scan across the pinch point at 002), as discussed in this work.

A. Structure factor of spin ice

In spin ice, the structure factor tensor $S^{\alpha\beta}(\mathbf{q})$ is characterized by two eigenvalues, longitudinal and transverse (to $\mathbf{q}$), here denoted by S^{L} and S^{T}, respectively. Polarized neutron scattering is required to fully characterize the correlations as it can separate these two functions, which in unpolarized neutron scattering appear in combination [11].

Here we define $\mathbf{Q} = \mathbf{q} + \mathbf{G}$, where $\mathbf{Q}$ is the scattering vector and $\mathbf{G}$ is a reciprocal lattice vector [Fig. 1(c)]. The neutron scattering differential cross section measures the transverse projection of the structure factor on the scattering vector [47]

$$\frac{d\sigma^{\alpha\beta}}{d\Omega} = A(\delta_{\alpha\beta} - \hat{Q}_\alpha \hat{Q}_\beta) S^{\alpha\beta}(\mathbf{Q}) \qquad (2)$$

(we set $A = 1$ henceforth). With the caveat discussed in the Appendix, Sec. 1, which is unimportant here, the structure factor is the same in each Brillouin zone [hence characterized as $S^{\alpha\beta}(\mathbf{q})$], but its projection may vary from zone to zone, as seen in Figs. 1(b) and 1(c).

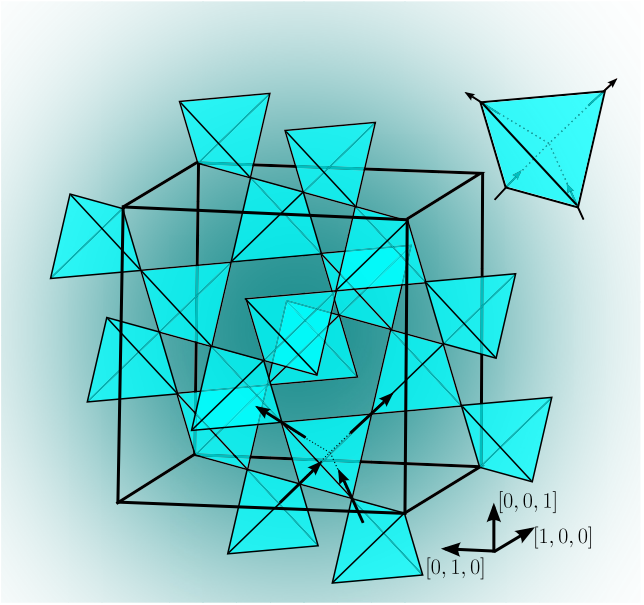

FIG. 2. Conventional cubic unit cell of the pyrochlore lattice consisting of 16 lattice sites (corners of the tetrahedra are the sites). The spins reside on the corners of the tetrahedra and their respective lattice vectors are pinned to the local $\langle 111 \rangle$ directions due to the nature of the crystal fields. A spin thus points towards the center of one tetrahedron while pointing away from the center of another and vice versa. The inset (top right) shows that the ground state of spin ice consists of a spin configuration for which each tetrahedron exhibits two spins pointing in and two spins pointing out.

The origin of the pinch points may be visualized by representing the inverse of the tensor $S^{\alpha\beta}(\mathbf{q})$ as an ellipsoid of dimensions $\sqrt{S^{\mathrm{L}}(\mathbf{q})} \times [\sqrt{S^{\mathrm{T}}(\mathbf{q})}]^2$, oriented with the principal (L) axis parallel to $\mathbf{q}$ [48,49]. In a dipolar ferromagnet, say, the ellipsoid is eccentric, i.e., $S^{\mathrm{L}} \neq S^{\mathrm{T}}$, only at small q [2], but in spin ice, the conspiracy of ice rules and very strong dipolar forces impose a nonspherical structure factor tensor over nearly the entire Brillouin zone [48]. Considering the in-plane projection of this ellipsoid on $\mathbf{Q}$ [Fig. 1(c)], the pattern shown in Fig. 1(b) is easily inferred. If the ellipsoid remains eccentric as $q \to 0^+$ then the pinch points are infinitely sharp; if it evolves to a sphere in that limit they are broadened [Fig. 1(c)]. Precisely at $q = 0$, in either case, the structure factor ellipsoid is a sphere, in accord with the crystal symmetry. In physical terms, the sharpness of the pinch points gives a highly sensitive measure of the screening of fields at long distance, as discussed subsequently.

We focus on the case of $\mathbf{G} = 002$ in the $1\bar{1}0$ scattering plane used in the experiments [11,12]. If we inspect wave vectors $\mathbf{Q} = hh(l = 2)$ within the 002 zone, then $h\bar{h}0$ and $hh0$ define two principal axes of the tensor [Fig. 1(d)]. Non-spin-flip (NSF) scattering then measures the out-of-plane transverse (to $\mathbf{q}$) eigenvalue, while spin-flip (SF) scattering measures a mixture of longitudinal and transverse eigenvalues in plane; with the projection perpendicular to $\mathbf{Q}$, this mixture creates the pinch points in the SF channel [Fig. 1(b)], while the NSF scattering, as a pure eigenvalue, remains a periodic function. However, it turns out (see the Appendix, Sec. 1) that a SF scan along $hh2$ picks out only the longitudinal eigenvalue

up to about $h = 0.5$, so this particular scan "across" the pinch point isolates the two eigenvalues needed to characterize the correlations in spin ice: S^{L} in the SF channel and S^{T} in the NSF channel. Thus, except very near the zone boundary, the entire correlation function of spin ice is contained in the two channels (SF and NSF) of the single line scan across the 002 zone center in the $1\bar{1}0$ scattering plane.

B. Plan and summary of the paper

In this paper we ask whether the pinch points of spin ice are broad or sharp [see Fig. 1(c)] and what physics the answer reveals. We discuss this with respect to high-resolution numerical simulations of NNSI and DSI, as well as with respect to existing experimental data [11,12] and analytical theories [13,14].

The paper is organized as follows. In Sec. II we describe details of our numerical simulations. In Sec. III we present an analytical theory of the correlations of NNSI that perfectly captures the simulated pinch point profile. In Sec. IV we extend this model to dipolar spin ice by including the long-range dipole interactions and show how the (the hitherto broad) pinch points become infinitely sharp, consistent with existing theory [13,14]. This is indicative of unscreened fields. As a contrast, in Sec. V we consider the corresponding model of fully screened dipolar fields, which leads to broad pinch points but is ruled out by the simulations. In Sec. VI we compare these results with the results of polarized neutron scattering experiments [11,12]. The experimental data are shown to be quantitatively described by the screened theory, rather than by the unscreened theory that describes the dipolar spin ice simulation. This disagreement between theory and experiment follows logically from accepted premises and so has the character of a paradox: the pinch point paradox of our title. In Sec. VII we summarize and discuss our main results, including possible resolutions of the paradox.

II. NUMERICAL SIMULATIONS

In the spin ice materials $R_2Ti_2O_7$, rare-earth ions R = Ho or Dy are located on the points of a cubic pyrochlore lattice of corner-sharing tetrahedra [50] (see Fig. 2). The trigonal crystal field enforces a doublet ground state for each ion [51–54] and establishes a local Ising-like [54] confinement with effective two-state spins $\mathbf{S}_i$ pointing between the centers of each pair of adjacent tetrahedra. The associated magnetic moments are very large, $\mu \approx 10\,\mu_{\mathrm{B}}$, with the consequence that dipole-dipole interactions are particularly strong in these materials. For modeling purposes we consider classical spins of unit length. The dipolar spin ice model combines the long-range dipolar interaction with short-range exchange terms [34]:

$$\mathcal{H} = J_1 \sum_{\langle i,j \rangle} \mathbf{S}_i \cdot \mathbf{S}_j + Da^3 \sum_{i>j} \frac{\mathbf{S}_i \cdot \mathbf{S}_j - 3(\hat{\mathbf{r}}_{ij} \cdot \mathbf{S}_i)(\hat{\mathbf{r}}_{ij} \cdot \mathbf{S}_j)}{r_{ij}^3}. \tag{3}$$

Here D is the dipolar interaction constant, r_{ij} the distance between spins i and j, and J_1 the nearest-neighbor exchange interaction [33]. Considering only nearest-neighbor interactions, the model reduces to the NNSI model, which gives an accurate approximation to DSI down to about 0.6 K [55]. The NNSI model has an effective ferromagnetic exchange parameter J_{eff}, which takes the values 1.1 K for $Dy_2Ti_2O_7$ and 1.9 K for $Ho_2Ti_2O_7$ [33]. The NNSI model maps exactly [32] to Pauling's model of (cubic) water ice [28], based on the Bernal-Fowler ice rules [56]. Hence it exhibits a degenerate ground state with strong correlations, but no long-range order (see Fig. 2). By introducing the dipolar interaction, the degeneracy of the NNSI model is weakly broken and an ordering transition at very low temperature is induced. However, this is not relevant at the temperatures ($T > 1$ K) considered in this paper, where DSI behaves qualitatively like NNSI. In addition to the nearest-neighbor exchange interactions J_1, the generalized spin ice model contains second- and third-nearest-neighbor interactions J_2, J_{3a}, and J_{3b}. A set of parameter values was previously determined for $Dy_2Ti_2O_7$ ($J_1 = 3.41$ K, $J_2 = -0.14$ K, and $J_{3a} = J_{3b} = 0.025$ K) which models unpolarized neutron scattering and bulk thermodynamic properties at a quantitative level [35].

We previously reported that demagnetizing effects are a pure outcome of dipolar interactions in highly correlated systems [57], i.e., the exchange interactions do not alter the shape-dependent physics at the zone center. Nevertheless, the diffuse scattering elsewhere in the Brillouin zone may depend upon exchange, as discussed subsequently. To model the neutron structure factor in more detail, we reconstruct the Fourier transform of the spin-spin correlation function in $\mathbf{Q}$ space. Following the use of a parallel Monte Carlo code [30] that exploits the symmetry of the dipolar interactions [58], we use periodic Ewald boundary conditions [58] and a loop algorithm [59] to speed up equilibration when needed at low temperature.

The surface dependence is treated via spherical boundary conditions by considering the addition of a microscopic term to the Ewald sum [60,61]. The choice of this boundary term is the foundation of the conditional convergence of the dipolar sum and exploits a way to manage the demagnetizing effects.

High resolution is key to this study. The allowed $\mathbf{Q}$ points were determined by considering only the set of points in which the discrete Fourier transform is defined, i.e., the inverse cubical system size $1/L$. For example, the high resolution of $L = 16$ which we reach corresponds to 65 536 particles and a resolution of $1/L = 0.0625$ in units of 2π. Considering that the dipolar systems under study occupy an ordered lattice, parallel computing is essential, given that a system of 65 536 particles corresponds to almost 4.3×10^9 interactions per Monte Carlo step. Note that we do not employ any interpolation schemes such as the Nyquist-Shannon sampling theorem as this would defeat our purpose of establishing the actual line shapes and their comparison with experiment.

III. NEAR-NEIGHBOR SPIN ICE

In this section we derive closed-form analytical expressions for the eigenvalues of the structure factor tensor $S^{\alpha\beta}(\mathbf{Q})$ of NNSI and compare them with our simulations. As justified in the Appendix, Sec. 1, the theory presented below assumes a continuum magnetization $\mathbf{M}(\mathbf{r})$. We consider a cut through the $\mathbf{G} = 002$ zone center such that $\mathbf{q} = hh0$ in reduced units. Defining θ as the angle between $\mathbf{Q}$ and $\mathbf{G}$, it is shown in

the Appendix, Sec. 1 that up to $h \approx 0.5$, the SF and NSF channels measure the longitudinal and transverse eigenvalues of the magnetization structure factor to an excellent approximation. We can therefore conveniently compare $d\sigma^{\rm NSF}_{hh2}/d\Omega$ with $S^{\rm T}_{hh0}$ and $d\sigma^{\rm SF}_{hh2}/d\Omega$ with $S^{\rm L}_{hh0}\cos^2\theta = 4S^{\rm L}_{hh0}/(4+2h^2)$ in this range.

Introducing the susceptibility χ and diffusion length ξ [14], the scattering function of NNSI may be calculated from the free-energy functional [62]

$$G[\mathbf{M}] = \mu_0 \int \left(\frac{\mathbf{M}^2}{2\chi} + \frac{\xi^2(\nabla\cdot\mathbf{M})^2}{2\chi} - \mathbf{H}\cdot\mathbf{M} \right) d^3r, \qquad (4)$$

which comes from an expansion of the free energy in powers of magnetization $\mathbf{M}$. Its first term in the susceptibility χ and its third term in the field $\mathbf{H}$ are common to all classical spin systems, while the second term in $(\nabla\cdot\mathbf{M})^2$ expresses the free-energy cost of divergence and is the lowest-order gradient term for ice systems [5,6]. The Euler-Lagrange equation $\mathbf{M} - \xi^2\nabla(\nabla\cdot\mathbf{M}) = \chi\mathbf{H}$ may be solved in Fourier components to give the wave-vector-dependent susceptibility $\chi(\mathbf{q})$ and, by the classical fluctuation dissipation theorem, the eigenvalues of the scattering tensor

$$S^{\rm T}(q) = \chi T/3C, \quad S^{\rm L}(q) = \frac{\chi T/3C}{1+\xi^2 q^2}. \qquad (5)$$

Here T (L) indicates transverse (longitudinal) to the wave vector $\mathbf{q}$.

The susceptibility may be expressed as $\chi = \gamma(T)C/T$, with $C = \mu_0 m^2/(3k_{\rm B}v_0/2)$, where m is the rare-earth moment and $v_0 = v/2$ is the volume per tetrahedron. The moment is related to the monopole charge Q by $Q = 2m/a$, where a is the diamond lattice constant [37]. The factor $\gamma(T)$ has been calculated by Jaubert *et al.* [63] in a Husimi tree approximation

$$\gamma(T) = \chi T/C = \frac{2(1+e^{2J_{\rm eff}/T})}{2+e^{2J_{\rm eff}/T}+e^{-6J_{\rm eff}/T}}, \qquad (6)$$

where $J_{\rm eff}$ is the effective exchange defined above [33].

The diffusion length $\xi(T)$ depends on the densities of single and double charge monopoles (which have no Coulomb interaction in NNSI). We make a low-temperature approximation by setting the chemical potential of the double-charge monopoles infinite. We write the entropy [36,41] in terms of the densities of positive and negative monopoles, pick out a component of the free energy $G = -\mu n_+ - \mu n_- - TS$ (where $\mu = -2J_{\rm eff}$ is the monopole chemical potential), and then substitute $n_+ \to (n+\delta_n)/2$ and $n_- \to (n-\delta_n)/2$, where n is the equilibrium monopole density and δ_n a fluctuation. A Taylor expansion of the free energy in powers of δ_n, followed by setting the linear term to zero, gives the equilibrium density [36]

$$n = \frac{4e^{-2J_{\rm eff}/T}}{3+4e^{-2J_{\rm eff}/T}} \qquad (7)$$

and a second-order fluctuation term $G'' = \mu_0 kT(\delta_n)^2/2nv_0$. The latter may be related to Eq. (4) using $(\delta_n)^2 = (\nabla\cdot\mathbf{M})^2/(Q/v_0)^2$ to give [62]

$$\xi^2 = \frac{\chi kT v_0}{\mu_0 Q^2 n}. \qquad (8)$$

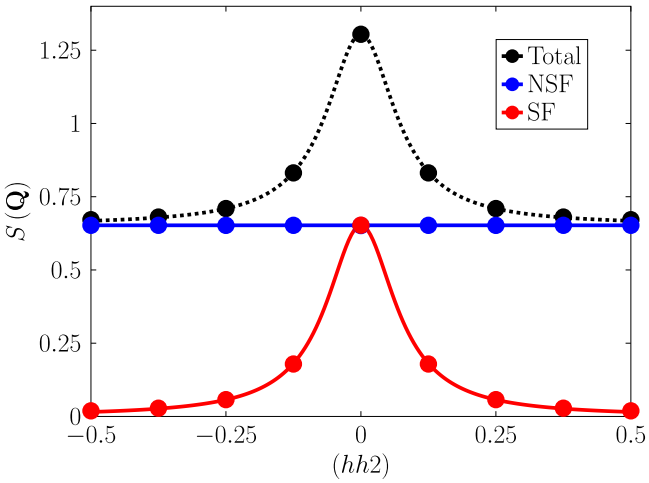

FIG. 3. Test of the accuracy of our analytic theory of (NNSI) (periodic boundary conditions). Shown is the pinch point profile at $T = 1$ K with $Ho_2Ti_2O_7$ parameters. Results of the numerical simulation (points) are shown versus those of the analytical theory developed in this paper (lines). The comparison of analytical theory and simulation is observed to be essentially perfect.

Equations (5)–(8) combine to give an analytic calculation of the full scattering function tensor. This is a low-temperature approximation: For $Ho_2Ti_2O_7$ parameters ($2J_{\rm eff} = -\mu = 3.8$ K), it should be valid at $T = 2$ K and below, where double-charge monopoles are very scarce.

In Fig. 3 we compare the calculated scattering functions of NNSI with the numerically simulated one: The parameter-free comparison is excellent, showing that the continuum theory is a nearly exact description of NNSI over the wave vectors considered. This gives us great confidence that the theory can be adapted to describe DSI as well. It is noteworthy that use of the continuum Laplacian ($-q^2$), rather than a lattice Laplacian, is sufficient to describe the data, which validates our continuum description.

IV. DIPOLAR SPIN ICE

Given the excellent comparison of theory and simulation for NNSI (preceding section), we seek to describe DSI by a natural extension of the NNSI theory. In particular, we simply add a term to Eq. (4) to describe the magnetostatic energy

$$U_{\rm mag} = -\frac{\mu_0}{2}\int \mathbf{M}\cdot\tilde{\mathbf{H}}\, d^3r, \qquad (9)$$

where $\tilde{\mathbf{H}}(\mathbf{r})$ represents the local internal far field arising from the dipoles at points $\mathbf{r}'$ in the sample. Treating $\tilde{\mathbf{H}}$ as an independent variable, the Euler-Lagrange equation becomes

$$\mathbf{M} - \xi^2\nabla(\nabla\cdot\mathbf{M}) = \chi(\mathbf{H}+\tilde{\mathbf{H}}), \qquad (10)$$

which can be solved for the structure factor as above if $\tilde{\mathbf{H}}$ can be expressed as a function of $\mathbf{M}$.

It is well known (see, for example, Ref. [64]) that the field at a point external to a system of dipoles (e.g., at $\mathbf{r}$ where the dipoles are at $\mathbf{r}'$) may be expressed as a sum over the fields arising from surface magnetic charge density

$\sigma = \mathbf{M}\cdot\hat{\mathbf{n}}$ (where $\hat{\mathbf{n}}$ is the unit vector normal to the surface) and volume magnetic charge density $\rho = -\nabla\cdot\mathbf{M}$. Without yet being explicit about surface effects, we write

$$\tilde{\mathbf{H}}(\mathbf{r}) = -\frac{\mu_0}{4\pi}\nabla\int\frac{\rho(\mathbf{r}')}{|\mathbf{r}-\mathbf{r}'|}d^3r'. \tag{11}$$

By the Helmholtz theorem, the dipolar field is then equal to the irrotational (longitudinal) component of the magnetization $\tilde{\mathbf{H}} = -\mathbf{M}^{\mathrm{L}}$. Writing $\mathbf{M} = \mathbf{M}^{\mathrm{L}} + \mathbf{M}^{\mathrm{T}}$ thus renders the dipolar correction entirely local and we may proceed as above to find the structure factors

$$S^{\mathrm{T}} = \gamma/3, \quad S^{\mathrm{L}} = \frac{\gamma/3}{(1+\chi)+q^2\xi^2}. \tag{12}$$

These are the same as Eq. (5) but with the longitudinal structure factor suppressed by a factor $1/(1+\chi)$ at the zone center. Also, the characteristic length becomes the Debye length $\xi/\sqrt{1+\chi}$ rather than the diffusion length ξ [14]. In addition [not shown in Eq. (12)], there is a δ function at the zone center; this is elucidated for the case of different boundary conditions in the Appendix, Sec. 2.

It has been shown [48] that treating the dipolar field in this way is equivalent to Onsager's cavity construction [65] for dipolar fields, where the magnetic charge resides on the surface of a spherical cavity cut in a continuous polarizable medium. Alternatively, we can see that the dipolar integral is equivalent to a discrete summation over the effective magnetic monopoles of spin ice. These two different physical pictures give the same result only if the fields are unscreened [48]. Hence we refer to this as the unscreened model going forward.

Following Eq. (A4) and the discussion thereafter, we may once again compare $d\sigma^{\mathrm{NSF}}_{hh2}/d\Omega$ with S^{T}_{hh0} and S^{SF}_{hh2} with $S^{\mathrm{L}}_{hh0}\cos^2\theta$ up to $h = 0.5$. Figure 4 compares the DSI simulation with the unscreened dipolar calculation at $T = 2$ K. We see that the simulated SF scattering function is immediately well described by the unscreened model, the NSF slightly less well. Since χ is large, e.g., $\chi \approx 6$ at $T = 2$ K [66], the Lorentzian peak becomes very broad and flat compared to that of NNSI.

There are two small modifications to the unscreened model that are worth considering. First, we notice that the NSF scattering is better described by $S^{\mathrm{T}} \sim 2/3 - S^{\mathrm{L}}$ (see Fig. 4). As discussed in Ref. [48], this correction is both plausible, because it satisfies the total moment sum rule, and justifiable, because the longitudinal fields were altered independently of the transverse. Second, the scattering function (A9) apparently depends on $2J_{\mathrm{eff}}$ rather than the magnetic monopole chemical potential, which, for dipolar spin ice, exceeds $2J_{\mathrm{eff}}$ in magnitude owing to the Coulomb interaction between monopoles. This difference increases the equilibrium defect density n, altering the specific heat [41]. As Eq. (A9) depends on n through ξ [Eqs. (7), (8), and (A9)], it might be appropriate to replace n by the true equilibrium density [41]. A fit to the ensuing function is tested in Fig. 4, but in fact it makes the description of the DSI simulation slightly poorer.

V. SCREENED MODELS

In the preceding section it was shown that high-resolution numerical simulations of the pinch points in dipolar spin ice do *not* evidence the deconfined and screened magnetic charge expected of magnetic monopole theory [37]. In the Appendix, Sec. 2 we show that the same theoretical result may be recovered from Debye-Hückel theory of magnetic monopoles, by tending the inverse monopole screening length κ to zero while keeping the Debye length fixed. This is a surprise because it is well established from analysis of the specific heat that monopoles are screened with a finite κ [41] equal to the inverse Debye length. However, it was shown in Ref. [14] that the monopole potential ϕ consists of both a screened part and an unscreened part (see Fig. 5) (this feature was also noted as a dipolar tail in the correlation function in Ref. [13]). The energy and hence specific heat is determined by the short-range screened part of the potential, whereas the pinch point is determined by the long-range unscreened part. An analysis based on the Poisson-Boltzmann equation (see the Appendix, Sec. 2) forces the potential into a perfectly exponential decay. Hence Debye-Hückel theory can only describe the pinch point if the screening length κ^{-1} is set to be infinite, recovering the Poisson equation. In contrast, to calculate the specific heat [41], it incurs a negligible error to neglect the power-law tail of the potential, and equate κ with the Debye length of the monopole fluid.

We also show in the Appendix, Sec. 2 how the inverse screening length κ and defect correlation length ξ may be treated in phenomenological terms, as independent parameters in a generalized theory. Suppression of screening ($\kappa \to 0$ at finite ξ) yields the unscreened model that captures the numerical simulation, while setting κ to the Debye-Hückel parameter for single- and double-charge magnetic monopoles (as calculated in Ref. [41]) and $\xi = 0$ results in a different physical picture. This consists of dipoles screened by

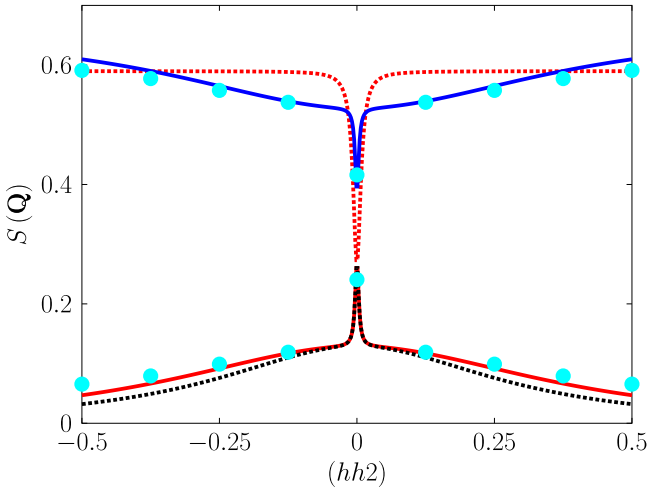

FIG. 4. Dipolar spin ice at $T = 2$ K with $Ho_2Ti_2O_7$ parameters and spherical boundary conditions. A comparison of the numerical simulation (points) and the unscreened analytical theory presented in this paper (lines) is shown. Red lines show the unmodified analytical theory (12). The blue line is the NSF scattering generated with $S^{\mathrm{T}} \sim 2/3 - S^{\mathrm{L}}$ (see the text). The dotted line shows the result using the monopole density replacing the bare defect density (see the text). The figure shows that the simplest possible extension of the near-neighbor spin ice theory to include dipolar interactions captures the numerical data to a close approximation.

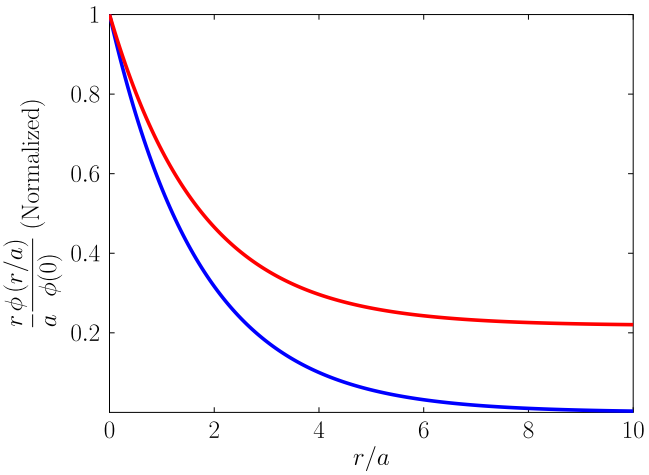

FIG. 5. Magnetic monopole potential calculated using $Ho_2Ti_2O_7$ parameters at $T = 2$ K. The figure shows $r\phi(r)$ normalized to its value at $r = 0$ (here a is the lattice constant of the diamond lattice inhabited by the monopoles [37]). The blue line is the standard Debye-Hückel potential $\phi(r) \sim e^{-r}/r$, which is screened to zero at long distance. The red line is the monopole potential in spin ice [14], revealing a power-law tail $\phi(r) \sim 1/r$ and hence an unscreened contribution at long distance. The unscreened contribution is the cause of the infinitely sharp pinch points in dipolar spin ice. It is confirmed in simulation (Fig. 4) but is not observed in experiment (Sec. VI).

deconfined monopoles, the model of Ref. [48], which we refer to as the screened dipolar fluid model, or screened model for short; it is essentially a two-fluid model of dipoles coexisting with deconfined charge. A comparison of the line shapes of the two limiting cases is given in Fig. 6. The key difference is that the screened model has a broadened pinch point and an inverse Lorentzian dip in the transverse channel.

To confirm that the simulated pinch point is truly sharp, we examine the simulation at a much higher temperature (10 K) where κ should be sufficiently large to make the central Lorentzian (broadened δ function) easily visible within the

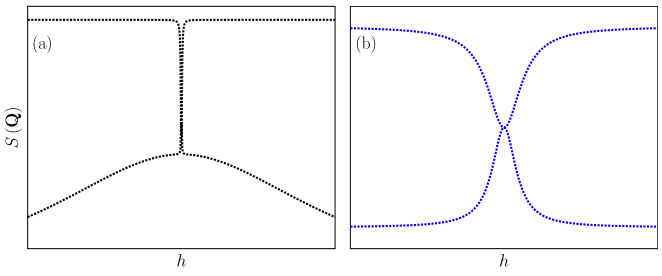

FIG. 6. Limiting line shapes in our more general analytical theory that allows for screening of dipolar fields by the magnetic charge density. (a) Case of infinite screening length ($1/\kappa = \infty$) and finite defect diffusion length ξ. (b) Case of finite screening length ($1/\kappa$) and zero diffusion length $\xi = 0$. It can be seen that the screening length $1/\kappa$ controls the sharpness of the central peak, while the defect diffusion length controls the flatness of the background. The completely flat background in the right-hand feature corresponds to the harmonic phase of Ref. [48].

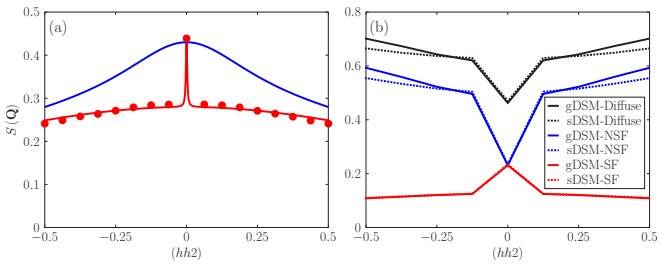

FIG. 7. (a) High-resolution simulation of DSI at $T = 10$ K to test for the sharpness of the central peak component. Points show the simulated data. The lower line is the unscreened line shape and the upper line is the corresponding NNSI line shape for comparison. There is no broadening of the central peak within the resolution of the simulation. (b) Comparison of simulations of the dipolar spin ice model with a single exchange constant (*s*DSM) with the generalized dipolar model (*g*DSM) ($Dy_2Ti_2O_7$ parameters [35]). Simulated points spaced by 0.125 are linked by solid lines as guides to the eye. Differences between the *s*DSM and *g*DSM are observed to be confined to the wings of the scan, showing that the detailed tuning of short-range exchange constants does not significantly affect the pinch point profile near the zone center.

resolution of our simulation. The result, shown in Fig. 7, does indeed rule out any pinch point broadening on the expected scale. (Note that, to obtain the fit to the unscreened model, we adjusted ξ slightly to account for double-charge monopoles.) Our simulation rules out the screened dipolar fluid model although the harmonic phase (flat background) of Ref. [48] is present to a certain approximation, given that the diffusion Lorentzian is very broad and flat at higher temperatures.

VI. PINCH POINT PARADOX

The pinch point line shape of polarized neutron scattering in $Ho_2Ti_2O_7$ spin ice has been independently studied by Fennell *et al.* [11] and by Chang *et al.* [12]. Both sets of authors found that it can be described by a central Lorentzian plus a temperature-dependent flat, i.e., q-independent, component at all temperatures. An explanation of the flat component was put forward by one of us in Ref. [48] in terms of the screened dipolar fluid model described above, i.e., $\xi = 0$, finite κ as calculated in Ref. [41]. This quantitatively produced the observed temperature dependence of the flat component as well as producing a Lorentzian central peak (note that in subsequent figures, the "flat" background is not completely flat because of the $\cos^2\theta$ factor discussed above). However, the screened model of Ref. [48] is already ruled out as a model for the DSI simulations.

The essence of the pinch point paradox is shown in Fig. 8, where we compare the SF scattering at $T = 2$ K measured by Chang *et al.* [12] with the DSI simulation, and the screened and unscreened theories (the latter for $\xi = 0$, the dipolar fluid case [48]). The experimental data were scaled such that the $q = 0$ point is coincident with the theory, i.e., we assume that theory and experiment are consistent as regards the bulk susceptibility (this is an approximation, but a reasonably accurate one). We see very clearly that the experiment rules out the unscreened DSI but is remarkably well described by the screened dipolar fluid. Indeed, the screened line shape

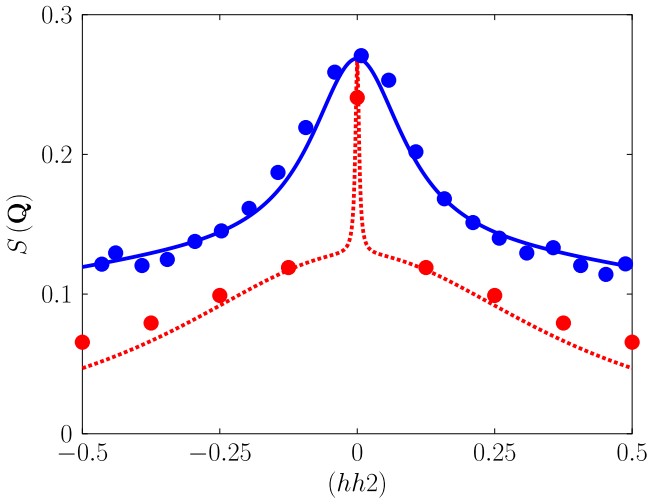

FIG. 8. Pinch point paradox in spin ice. A comparison of the experimental data and numerical data with the limiting forms of the analytical theory is shown. The SF data of Chang *et al.* [12] (blue circles) and our simulation (red circles, spherical boundary conditions) are shown at $T = 2$ K. The experimental data have been scaled to fit the theory (lines) at 002. The blue line is the screened theory and the red line the unscreened theory. The fact that experiment and simulation are only consistent with *different* limiting cases of the *same* analytical theory (Fig. 6) is the essence of the pinch point paradox.

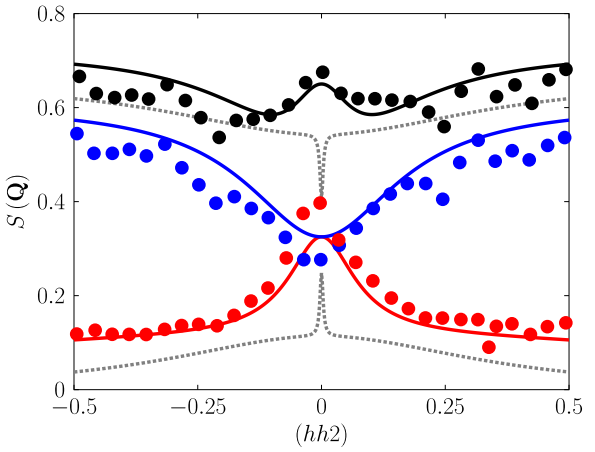

FIG. 9. Further comparison of the numerical data and limiting forms of the analytical theories at $T = 1.7$ K with the experimental SF (lower, red), NSF (middle, blue), and total (upper, black) data of Fennell *et al.* [11]. The red, blue, and black lines are the screened theory. The experimental data have been scaled such that the total scattering approximately fits the solid black line. The dotted black lines are the unscreened theory that has been shown to describe DSI extremely well (Fig. 4). It is concluded that numerics and experiments are again described by different limiting cases of the same theory (see Fig. 6). Note that the demagnetizing factor in the screened theory has been adjusted to better fit the data in the center of the scan (see the text).

can be transformed [48] into independent flat and Lorentzian components, where the Lorentzian component has the same width parameter as NNSI. This is in perfect agreement with the analysis of Chang *et al.*, who fitted these data using Monte Carlo simulations of NNSI plus an arbitrary flat background; our theory eliminates the adjustable parameter used by these authors. They also drew a central Lorentzian through the points of their simulations of DSI, a reasonable extrapolation in view of knowledge available at the time, but one that we have now shown to be incorrect through higher-resolution simulations. Because DSI has a δ function rather than a Lorentzian central peak, the discrepancy between simulation and experiment for spin ice is a very large one, yet both simulation and experiment should *a priori* be considered correct, hence the paradox.

In the case of the 1.7 K SF, NSF, and total neutron scattering data of Fennell *et al.* [11], the DSI again fails badly, while the screened dipolar fluid is again close to the experimental data (see Fig. 9; the fit has been improved slightly by adjusting the demagnetizing factor to 0.2). Notably, the screened dipolar fluid model captures the striking zone center dip in the SF scattering as well as the small zone center bump in the total scattering. In general, we found that the screened model outperforms the unscreened one at all temperatures, in every case describing the flat (harmonic phase) background well, though at higher temperatures overestimating the Lorentzian width by a significant factor, e.g., ∼5. Despite this, we can certainly conclude that, in the temperature range where we are most sure of the theory, the screened dipolar fluid model is fully consistent with experiment, while the DSI simulation and unscreened models are ruled out as descriptions of experiment.

VII. DISCUSSION

Our study exposes two significant results: (i) The pinch point profile in the dipolar spin ice simulation is infinitely sharp and (ii) experiment disagrees with simulation in that the profiles are broad, rather than sharp. Yet both are described quantitatively by different limits of the same theory.

To elaborate on (i), we recall that the subtle long-range correlations in spin ice are entirely revealed by neutron polarization analysis of the pinch point profile, as explained in the Introduction. In the near-neighbor spin ice model the pinch points are broad, but the addition of the long-range dipole-dipole interaction causes them to be infinitely sharp with a δ-function singularity at $q = 0$ [13,14]. The structure factor (inverse) tensor remains an oblate spheroid [see Figs. 1(c) and 1(d)], except precisely at $q = 0$, where it becomes a sphere, in keeping with the cubic space symmetry [49].

As dipolar spin ice represents a model Coulomb gas, this raises an interesting and topical point. The Debye length for magnetic monopole interactions ($=\xi/\sqrt{1+\chi}$) is always finite, and any long-range correction to the exponential screening is essentially negligible as regards monopole correlations or specific heat. However, the field-screening length ($=1/\kappa$) is, at the same time, *divergent*. Thus dipolar spin ice, a polarizable Coulomb gas that is relevant even as a model of water ice [67], presents a very different picture as regards charge correlations and field correlations: The screening length for fields diverges while the Debye length remains finite. This is not a contradiction as it depends on how a particular experimental measure picks out the details of what is a rather subtle and long-range correlation function [14] (see Fig. 5). In this context, we may make a connection with an interesting recent

discussion of the experimental observations of underscreening in dense ionic liquids [45,46]. We see that dipolar spin ice affords a tangible example where the screening length diverges, while the Debye length remain constant. This suggests that the observations of Refs. [45,46] may be consistent with the dense ionic liquid having a stable polarization.

To elaborate on (ii) we have constructed flexible theories of the line shape that accurately and quantitatively account for both our numerical results and the experimental results, but only, paradoxically, under different limits. Specifically, in experiment magnetic monopoles appear to screen the dipolar fields, leading to broad pinch points, while in simulation they do not screen, leading to sharp pinch points.

In seeking a resolution of the pinch point paradox, we believe that a first obvious possibility, pinch point broadening by structural defects and disorder in the samples, may immediately be discarded. Although real samples do contain defects and disorder (see Refs. [68–70] for a discussion of this and how to prepare defect-free samples), theory appears to rule this out as a cause of pinch point broadening. Thus, the role of defects and disorder has been considered theoretically in Ref. [13]. The case of nonmagnetic dilution was shown to lead to no broadening of the dipolar pinch points. Since our results agree with this theory in other respects, it therefore seems highly unlikely that a small concentration of defects and disorder in the experimental samples can give the very strong pinch point broadening that is actually observed.

We are also confident that a second obvious possibility, broadening by extra terms in the spin Hamiltonian, may also be ruled out. We have checked this by simulating the refined generalized DSI model (see Sec. II), which has been shown to give a most accurate description of $Dy_2Ti_2O_7$ [35]. We find differences with DSI only near zone boundaries (see Fig. 7). This is to be expected: In this dipolar paramagnet, only long-range, i.e., dipolar, interactions should affect the correlation function at small q. We also tested the dumbbell model [37] (as implemented in Ref. [71]), but found this to be qualitatively the same as DSI. We conclude with confidence that simple corrections to the classical model, or competition between short-range exchange and long-range dipolar forces (which can cause changes in the character of correlations in some systems [72]), are not implicated in the pinch point paradox.

Similarly, we have considered the possibility of various experimental corrections, but none of these give a convincing explanation of the paradox. For example, incomplete beam polarization, corrections to the static approximation, or other sources of background would not lead to the systematics that we observe. Finite instrumental resolution is always a potential source of broadening but can be largely ruled out here because the peak widths are much broader than the expected resolution and they are temperature dependent [11]. The fact that neutron data taken under different conditions on different instruments and sources are in excellent agreement further indicates that experimental corrections are not involved. It is also crucial to emphasize, as discussed above, that the analysis of Chang *et al.* of their data (Fig. 8) is quantitatively consistent with ours; this is a crucial proof that there is no inadvertent bias in our analysis (for example, a scaling of the experimental data onto one theoretical curve rather than the other in Fig. 8).

These considerations leave us to face the likelihood of more fundamental causes of the pinch point paradox, including quantum fluctuations, corrections to neutron scattering theory, and corrections to dipolar simulation methods.

A. Quantum fluctuations

We have treated spin ice here as a classical spin system, which is the accepted description of $Ho_2Ti_2O_7$ and $Dy_2Ti_2O_7$. However, there has been great interest recently in quantum spin ice and the possibility that it forms a quantum spin liquid state at low temperatures [73]. The key to formation of this state is the introduction of ring exchange, which leads to a quantum superposition of a hexagonal loops of spins in the Pauling state with its spin-reversed state [20,74–77]. Such ring exchange, and eventually the quantum spin liquid, can originate in anisotropic exchange terms that arise in higher orders of perturbation theory for the exchange-coupled rare-earth doublets (either Kramers or non-Kramers) [73]. Despite many complicating factors in experiment (not least the ubiquitous dipolar coupling) there is promising experimental evidence of quantum spin ice in several rare-earth pyrochlore materials (see Refs. [22,78,79] for recent examples). It has been shown by Benton *et al.* [20] that a key characteristic of quantum spin ice is a broadening and loss of the pinch point, qualitatively similar to what we observe. It has also been shown that this effect may survive the presence of dipolar coupling [80]. It is therefore worth asking if the pinch point paradox can be resolved by admitting quantum fluctuations into the hitherto classical description of the canonical spin ice materials. If that were the case we would have less of a paradox and more a simple disagreement of theory and experiment, requiring adjustment of the model.

On the one hand, there is strong experimental evidence of quantum superposed spin states in nominally classical spin ice. In particular, the superposition of spin-up and spin-down states associated with a monopole hop can be shown to give rise to a large isolated, i.e., quantum adiabatic, susceptibility at high frequency and this has been observed in experiment [43]. Hyperfine coupling can also cause tunneling between spin states [81]. On the other hand, it seems unlikely that such effects would give rise to appreciable ring exchange: As pointed out many years ago [32], the tunneling of hexagonal spin loops is hardly compatible with the low-temperature spin ice freezing observed experimentally. Theory also casts doubt on the possibility of quantum spin ice behavior in these materials: A careful appraisal of the theoretical problem [54] showed that the experimental systems considered here should approximate classical dipolar spin ice very closely.

On balance, we therefore think it unlikely that the broadening of the pinch point in the classical spin ices arises by the mechanism identified in Refs. [20,80], although we might add that stranger things have happened and more detailed theory, accounting for the dipole interaction and general sources of quantum fluctuations, would be very welcome.

B. Corrections to neutron scattering theory

The theory of neutron polarization analysis is well established following the pioneering work of Halpern and Holstein

[82] and Moon *et al.* [83]. It is customary to map the orbital contributions to the magnetic moment onto effective spin operators, but the experimental systems considered here have largely orbital, rather than spin, magnetism. We suggest it would be worth closely examining the polarization analysis theory for spin ice. For example, it is certain that there would be some degree of interaction of the neutron within the orbital dipole, i.e., with the self-field, and we speculate that this might have some effect on the structure factor. Similarly, we might imagine some rather complex depolarization effects in spin ice, but these would have to go well beyond the standard picture of depolarization to explain our observations.

C. Corrections to dipolar simulation method

Clearly, the method used agrees with experiment at large q and at $q = 0$, but does not do so at small but finite q. If we take the analytical theory to be a guide, we can expect the pinch point broadening to occur, regardless of the boundary conditions, so it would even be present for periodic (Ewald) boundaries. Although it seems most unlikely that a tried and tested method like Ewald summation would have some basic flaw, it is also unlikely that it has ever been subject to such a stringent experimental test, so this question is worth examining in much greater detail. In this context, it is worth emphasizing that the simulation does agree with experiment insofar as the total scattering or trace of the correlation function; the discrepancy is at the level of the Helmholtz decomposition or polarization analysis. As above, it would be worth reconsidering the role of self-field (the internal structure of the dipole) as an obvious point of difference between theory and experiment. It is not present in simulation, the demagnetizing effect being implemented via a demagnetizing tensor, but it remains a very real and potentially important [84] experimental property.

VIII. CONCLUSION

In conclusion, pinch points typify an important and widespread scattering feature in condensed matter. Topics of current theoretical interest include the coexistence of pinch points with ordered states [38,85,86], extensions of the pinch point concept [87,88], pinch points as a diagnostic of quantum fluctuations [20,89], and pinch points in Coulomb systems [90–93]. In general, a sharp pinch point indicates that the structure factor tensor remains eccentric as $q \to 0$, typically as a result of unscreened power-law correlations. These pinch points will broaden if the long-range correlations are exponentially damped, as occurs with the screening of long-range interactions. Using very-high-resolution dipolar simulations and by comparing to existing experiment, we have exposed an unusual paradox in dipolar spin ice: The dipolar fields are not screened in simulation but do appear to be screened in experiment.

From a purely theoretical perspective, the pinch point paradox may be summarized as follows. In the description of the experiment, the Poisson-Boltzmann equation for magnetic monopoles appears where the Poisson equation is expected; it is as if the magnetic monopoles of spin ice behave much more like "real charges" (Dirac monopoles) than expected [37].

ACKNOWLEDGMENTS

It is a pleasure to thank T. Fennell, P. C. W. Holdsworth, and C. Gray for many useful discussions and related collaborations and P. C. W. Holdsworth for critical comments on the manuscript. The simulations were performed on resources provided by the Swedish National Infrastructure for Computing at the Center for High Performance Computing at the Royal Institute of Technology. We gratefully acknowledge the NVIDIA Corporation for the donation of GPU resources. M.T. was supported by Stiftelsen Olle Engkvist Byggmästare (Grant No. 187-0013) with support from Magnus Bergvalls Stiftelse (Grant No. 2018-02701).

The authors declare no competing financial interests.

APPENDIX

1. Magnetization fluctuations

Here we show that the NSF and SF channels of the scan considered in the main paper, and in the experiments, measure transverse and longitudinal magnetization fluctuations, respectively. This is not a foregone conclusion because the glide symmetry that emerges in the $Fd\bar{3}m$ space group of spin ice means that, with respect to the face-centered-cubic reciprocal lattice $\{\mathbf{G}\}$, the function $S^{\alpha\beta}(\mathbf{Q})$ is modulated such that the unit cell in reciprocal space is doubled. Hence every second zone is inequivalent; for example, the function is different in the zones defined by $\mathbf{G} = 002\,004$. In associated work [60] we refer to zones like 002 as false zones and zones like 004 as true zones. The fact that there are two types of zones is the only reason that experiment can clearly resolve the pinch points in spin ice. At the true zone centers the nuclear Bragg peak has its full intensity and this will always obscure the subtle magnetic diffuse scattering, even in a polarized experiment. In contrast, at a false zone center, e.g., 002, the nuclear intensity is zero, making the magnetic diffuse scattering accessible to precise measurement. However, this advantage potentially comes at a price: At a false center $S^{\alpha\beta}(\mathbf{Q})$ is not necessarily a measure of magnetization fluctuations, the quantity of most immediate interest. Yet there is a fortunate crystallographic coincidence that renders this point irrelevant to the present study: Scans across the pinch point at 002 (surprisingly) do yield the magnetization fluctuations as required, as described subsequently.

The continuum approximation to the local magnetization used in our theory can only really be valid with respect to magnetization defined on a Bravais lattice such that a primitive unit cell can be defined which, on repetition, just fills all space. The pyrochlore lattice (Fig. 2) is a face-centered-cubic (F) Bravais lattice with a four-point tetrahedral basis. Hence $\mathbf{M}$ should be interpreted as the magnetization averaged over the four $\langle 111 \rangle$ spins of the spin ice basis

$$\mathbf{M} = g\mu_{\mathrm{B}} v^{-1} \sum_{i=1}^{4} \mathbf{s}_i, \tag{A1}$$

where g is the g factor, v is the primitive unit cell volume, and the spins

$$\mathbf{s}_1 = (1/\sqrt{3})(1, 1, 1),$$

$$\mathbf{s}_2 = (1/\sqrt{3})(-1, -1, 1),$$

$$\mathbf{s}_3 = (1/\sqrt{3})(1, -1, -1),$$
$$\mathbf{s}_4 = (1/\sqrt{3})(-1, 1, -1) \quad \text{(A2)}$$

are located at

$$\mathbf{r}_1 = (0, 0, 0),$$
$$\mathbf{r}_2 = (1/4, 1/4, 0),$$
$$\mathbf{r}_3 = (0, 1/4, 1/4),$$
$$\mathbf{r}_4 = (1/4, 0, 1/4), \quad \text{(A3)}$$

respectively, in the conventional cubic unit cell. It is straightforward to demonstrate that with respect to the axes $x = [1\bar{1}0]$, $y = [110]$, and $z = [001]$, the structure factors probed in the NSF and SF channels, S^{xx} and S^{yy}, measure the fluctuations $\langle M^x(\mathbf{q})M^x(-\mathbf{q})\rangle$ and $\langle M^y(\mathbf{q})M^y(-\mathbf{q})\rangle$, respectively. Because 002 is a false zone center (discussed above) this is not true of the third (zz) component. The difference arises because the zz structure factor samples fluctuations of four spins per tetrahedron in the combination $\sqrt{1/3}(s_1^z + s_2^z - s_3^z - s_4^z)$, which is not the same as M^z, while the xx and yy structure factors sample two spin combinations, e.g., $\sqrt{2/3}(s_1^x + s_2^x)$ and $\sqrt{2/3}(s_3^y + s_4^y)$, which are the same as the corresponding projections of M^x and M^y (this is because two of the spins in each case have zero component on the given axes x and y). We focus on a cut through the $\mathbf{G} = 002$ zone center such that $\mathbf{q} = hh0$ in reduced units and the observed differential cross sections are

$$\frac{d\sigma_{hh2}^{\mathrm{NSF}}}{d\Omega} = S_{hh0}^{xx},$$
$$\frac{d\sigma_{hh2}^{\mathrm{SF}}}{d\Omega} = S_{hh0}^{yy}\cos^2\theta + S_{hh0}^{zz}\sin^2\theta, \quad \text{(A4)}$$

where θ is the angle between $\mathbf{Q} = \mathbf{G} + \mathbf{q}$ and $\mathbf{G} = 002$. Fortunately, the phase factors of the zz component act to suppress the second term in Eq. (A4) such that it may be neglected up to $h \approx 0.5$. The net result is that the SF and NSF channels measure the longitudinal and transverse eigenvalues of the magnetization structure factor to an excellent approximation. We can therefore conveniently compare $d\sigma_{hh2}^{\mathrm{NSF}}/d\Omega$ with S_{hh0}^{T} and $d\sigma_{hh2}^{\mathrm{SF}}/d\Omega$ with $S_{hh0}^{\mathrm{L}}\cos^2\theta = 4S_{hh0}^{\mathrm{L}}/(4 + 2h^2)$ in this range.

2. Boundary conditions and screened models

To account for different boundary conditions, we add a self-field [84] to the dipolar field which generates the correct average when the field is summed over a ellipsoidal volume; in this way the demagnetizing factor N_{d} (=1/3 and 0 for spherical and Ewald boundaries, respectively) naturally enters the equations, obviating the need to treat surface charge explicitly. This factor is conveniently introduced by treating the dipolar integral as a sum over thermally generated monopoles and allowing these to screen each other as in a Debye-Hückel gas [41]. In this approximation, the dipolar field is not simply equal to negative $\mathbf{M}^{\mathrm{L}}$, but in addition has a longer-range harmonic component. At the very least, such a component is expected from the demagnetizing field that arises from the surface charge (surface monopoles). It was suggested in Ref. [48] that it could also arise from thermally generated monopoles at mesoscopic distances [48], although that is ruled out here for dipolar spin ice (see the main text).

We first consider the Debye-Hückel equation for the potential ϕ,

$$\nabla \cdot \nabla\phi(\mathbf{r}) + \kappa^2\phi(\mathbf{r}) = 0, \quad \text{(A5)}$$

which applies outside a region of size $\sim a$ at the origin. By taking the gradient of this equation and introducing a δ function to extend it to the origin we find, for the field at all $\mathbf{r}$,

$$-\nabla[\nabla \cdot \tilde{\mathbf{H}}(\mathbf{r})] - \kappa^2\tilde{\mathbf{H}}(\mathbf{r}) = [\nabla(\nabla \cdot \mathbf{M}) + \kappa^2 N_{\mathrm{d}}\mathbf{M}(\mathbf{r})]\delta(\mathbf{r}), \quad \text{(A6)}$$

where $-N_{\mathrm{d}}\mathbf{M}(\mathbf{r})\delta(\mathbf{r})$ is the self-field. The Debye-Hückel solution $\kappa \to \kappa_{\mathrm{DH}}$ then gives the Green's function solution for the more general equation where charge density is widely spread:

$$-\nabla[\nabla \cdot \tilde{\mathbf{H}}(\mathbf{r})] - \kappa^2\tilde{\mathbf{H}}(\mathbf{r}) = \int \{\nabla[\nabla \cdot \mathbf{M}(\mathbf{r}')] + \kappa^2 N_{\mathrm{d}}\mathbf{M}(\mathbf{r}')\}\delta(\mathbf{r} - \mathbf{r}')d^3r'. \quad \text{(A7)}$$

In Fourier components the field becomes

$$\tilde{\mathbf{H}}(\mathbf{q}) = -\{\mathbf{q}[\mathbf{q} \cdot \mathbf{M}(\mathbf{q})] + \kappa^2 N_{\mathrm{d}}\mathbf{M}(\mathbf{q})\}/(\kappa^2 + q^2) \quad \text{(A8)}$$

and the solution of the Euler-Lagrange equation is then

$$S^{\mathrm{L}} = \frac{(\gamma/3)(\kappa^2 + q^2)}{\kappa^2(\chi N_{\mathrm{d}} + 1) + q^2(1 + \chi + \kappa^2\xi^2) + q^4\xi^2}, \quad \text{(A9)}$$

$$S^{\mathrm{T}} = \frac{(\gamma/3)(\kappa^2 + q^2)}{\chi\kappa^2 N_{\mathrm{d}} + (\kappa^2 + q^2)}. \quad \text{(A10)}$$

Setting $\kappa \to 0$ in Eq. (A9) results in the unscreened scattering functions (12). In Fig. 4, to compute the scattering functions, we left κ small but finite, which broadens the δ function slightly to render it visible to the eye. Referring to Eq. (A9), varying κ and ξ finally generates a family of curves, as illustrated in Fig. 6.

[1] M. A. Krivoglaz, Effect of long-range forces on fluctuations and the scattering of waves in crystals, Fiz. Tverd. Tela. **5**, 3439 (1963) [Sov. Phys. Solid State **5**, 2526 (1964)].

[2] J. Als-Nielsen, L. M. Holmes, and H. J. Guggenheim, Experimental Test of Renormalization Group Theory on the Uniaxial, Dipolar Coupled Ferromagnet $LiTbF_4$, Phys. Rev. Lett. **37**, 1161 (1976).

[3] G. L. Paul, W. Cochran, W. J. L. Buyers, and R. A. Cowley, Ferroelectric transition in KD_2PO_4, Phys. Rev. B **2**, 4603 (1970).

[4] S. Havlin, R. A. Cowley, and H. Sompolinsky, Anisotropic polarization fluctuations in KD_2PO_4-type crystals, J. Phys. C **15**, 6057 (1982).

[5] R. Youngblood and J. D. Axe, Neutron-scattering study of short-range order in a model two-dimensional ferroelectric, Phys. Rev. B **17**, 3639 (1978).

[6] R. Youngblood, J. D. Axe, and B. M. McCoy, Correlations in ice-rule ferroelectrics, Phys. Rev. B **21**, 5212 (1980).

[7] V. M. Nield and R. W. Whitworth, The structure of ice I_h from analysis of single-crystal neutron diffuse scattering, J. Phys.: Condens. Matter **7**, 8259 (1995).

[8] B. Wehinger, D. Chernyshov, M. Krisch, S. Bulat, V. Ezhov, and A. Bosak, Diffuse scattering in I_h ice, J. Phys.: Condens. Matter **26**, 265401 (2014).

[9] R. Moessner and S. L. Sondhi, Theory of the [111] magnetization plateau in spin ice, Phys. Rev. B **68**, 064411 (2003).

[10] T. Fennell, S. T. Bramwell, D. F. McMorrow, P. Manuel, and A. R. Wildes, Pinch points and Kasteleyn transitions in kagome ice, Nat. Phys. **3**, 566 (2007).

[11] T. Fennell, P. P. Deen, A. R. Wildes, K. Schmalzl, D. Prabhakaran, A. T. Boothroyd, R. J. Aldus, D. F. McMorrow, and S. T. Bramwell, Magnetic Coulomb phase in the spin ice $Ho_2Ti_2O_7$, Science **326**, 415 (2009).

[12] L. J. Chang, Y. Su, Y.-J. Kao, Y. Z. Chou, R. Mittal, H. Schneider, T. Brückel, G. Balakrishnan, and M. R. Lees, Magnetic correlations in the spin ice $Ho_{2-x}Y_xTi_2O_7$ as revealed by neutron polarization analysis, Phys. Rev. B **82**, 172403 (2010).

[13] A. Sen, R. Moessner, and S. L. Sondhi, Coulomb Phase Diagnostics as a Function of Temperature, Interaction Range, and Disorder, Phys. Rev. Lett. **110**, 107202 (2013).

[14] M. I. Ryzhkin, I. A. Ryzhkin, and S. T. Bramwell, Dynamic susceptibility and dynamic correlations in spin ice, Europhys. Lett. **104**, 37005 (2013).

[15] P. W. Anderson, Ordering and antiferromagnetism in ferrites, Phys. Rev. **102**, 1008 (1956).

[16] T. Fennell, M. Harris, S. Calder, M. Ruminy, M. Boehm, P. Steffens, M. H. Lemee-Cailleau, O. Zaharko, A. Cervellino, and S. T. Bramwell, Multiple Coulomb phase in the fluoride pyrochlore $CsNiCrF_6$, Nat. Phys. **15**, 60 (2019).

[17] Y. Perrin, B. Canals, and N. Rougemaille, Extensive degeneracy, Coulomb phase and magnetic monopoles in artificial square ice, Nature (London) **540**, 410 (2016).

[18] E. Östman, H. Stopfel, I.-A. Chioar, U. B. Arnalds, A. Stein, V. Kapaklis, and B. Hjörvarsson, Interaction modifiers in artificial spin ices, Nat. Phys. **14**, 375 (2018).

[19] A. Farhan, M. Saccone, C. F. Petersen, S. Dhuey, R. V. Chopdekar, Y.-L. Huang, N. Kent, Z. Chen, M. J. Alava, T. Lippert, A. Scholl, and S. van Dijken, Emergent magnetic monopole dynamics in macroscopically degenerate artificial spin ice, Sci. Adv. **5**, eaav6380 (2019).

[20] O. Benton, O. Sikora, and N. Shannon, Seeing the light: Experimental signatures of emergent electromagnetism in a quantum spin ice, Phys. Rev. B **86**, 075154 (2012).

[21] T. Fennell, M. Kenzelmann, B. Roessli, M. K. Haas, and R. J. Cava, Power-Law Spin Correlations in the Pyrochlore Antiferromagnet $Tb_2Ti_2O_7$, Phys. Rev. Lett. **109**, 017201 (2012).

[22] R. Sibille, N. Gauthier, H. Yan, M. Ciomaga Hatnean, J. Ollivier, B. Winn, U. Filges, G. Balakrishnan, M. Kenzelmann, N. Shannon, and T. Fennell, Experimental signatures of emergent quantum electrodynamics in $Pr_2Hf_2O_7$, Nat. Phys. **14**, 711 (2018).

[23] M. P. Zinkin, M. J. Harris, and T. Zeiske, Short-range magnetic order in the frustrated pyrochlore antiferromagnet $CsNiCrF_6$, Phys. Rev. B **56**, 11786 (1997).

[24] P. H. Conlon and J. T. Chalker, Spin Dynamics in Pyrochlore Heisenberg Antiferromagnets, Phys. Rev. Lett. **102**, 237206 (2009).

[25] R. Ballou, E. Lelièvre-Berna, and B. Fåk, Spin Fluctuations in $(Y_{0.97}Sc_{0.03})Mn_2$: A Geometrically Frustrated, Nearly Antiferromagnetic, Itinerant Electron System, Phys. Rev. Lett. **76**, 2125 (1996).

[26] B. Canals and C. Lacroix, Quantum spin liquid: The Heisenberg antiferromagnet on the three-dimensional pyrochlore lattice, Phys. Rev. B **61**, 1149 (2000).

[27] C. L. Henley, Power-law spin correlations in pyrochlore antiferromagnets, Phys. Rev. B **71**, 014424 (2005).

[28] L. Pauling, The structure and entropy of ice and of other crystals with some randomness of atomic arrangement, J. Am. Chem. Soc. **57**, 2680 (1935).

[29] A. P. Ramirez, A. Hayashi, R. J. Cava, R. Siddharthan, and B. S. Shastry, Zero-point entropy in 'spin ice', Nature (London) **399**, 333 (1999).

[30] S. R. Giblin, M. Twengström, L. Bovo, M. Ruminy, M. Bartkowiak, P. Manuel, J. C. Andresen, D. Prabhakaran, G. Balakrishnan, E. Pomjakushina, C. Paulsen, E. Lhotel, L. Keller, M. Frontzek, S. C. Capelli, O. Zaharko, P. A. McClarty, S. T. Bramwell, P. Henelius, and T. Fennell, Pauling Entropy, Metastability, and Equilibrium in $Dy_2Ti_2O_7$ Spin Ice, Phys. Rev. Lett. **121**, 067202 (2018).

[31] M. J. Harris, S. T. Bramwell, D. F. McMorrow, T. Zeiske, and K. W. Godfrey, Geometrical Frustration in the Ferromagnetic Pyrochlore $Ho_2Ti_2O_7$, Phys. Rev. Lett. **79**, 2554 (1997).

[32] S. T. Bramwell and M. J. Harris, Frustration in Ising-type spin models on the pyrochlore lattice, J. Phys.: Condens. Matter **10**, L215 (1998).

[33] S. T. Bramwell and M. J. P. Gingras, Spin ice state in frustrated magnetic pyrochlore materials, Science **294**, 1495 (2001).

[34] B. C. den Hertog and M. J. P. Gingras, Dipolar Interactions and Origin of Spin Ice in Ising Pyrochlore Magnets, Phys. Rev. Lett. **84**, 3430 (2000).

[35] T. Yavors'kii, T. Fennell, M. J. P. Gingras, and S. T. Bramwell, $Dy_2Ti_2O_7$ Spin Ice: A Test Case for Emergent Clusters in a Frustrated Magnet, Phys. Rev. Lett. **101**, 037204 (2008).

[36] I. A. Ryzhkin, Magnetic relaxation in rare-earth oxide pyrochlores, J. Exp. Theor. Phys. **101**, 481 (2005).

[37] C. Castelnovo, R. Moessner, and S. L. Sondhi, Magnetic monopoles in spin ice, Nature (London) **451**, 42 (2008).

[38] M. E. Brooks-Bartlett, S. T. Banks, L. D. C. Jaubert, A. Harman-Clarke, and P. C. W. Holdsworth, Magnetic-Moment Fragmentation and Monopole Crystallization, Phys. Rev. X **4**, 011007 (2014).

[39] S. Petit, E. Lhotel, B. Canals, M. Ciomaga Hatnean, J. Ollivier, H. Mutka, E. Ressouche, A. R. Wildes, M. R. Lees, and G. Balakrishnan, Observation of magnetic fragmentation in spin ice, Nat. Phys. **12**, 746 (2016).

[40] C. Castelnovo, R. Moessner, and S. L. Sondhi, Debye-Hückel theory for spin ice at low temperature, Phys. Rev. B **84**, 144435 (2011).

[41] V. Kaiser, J. Bloxsom, L. Bovo, S. T. Bramwell, P. C. W. Holdsworth, and R. Moessner, Emergent electrochemistry in spin ice: Debye-Hückel theory and beyond, Phys. Rev. B **98**, 144413 (2018).

[42] V. Kaiser, S. T. Bramwell, P. C. W. Holdsworth, and R. Moessner, ac Wien Effect in Spin Ice, Manifest in Nonlinear, Nonequilibrium Susceptibility, Phys. Rev. Lett. **115**, 037201 (2015).

[43] L. Bovo, J. A. Bloxsom, D. Prabhakaran, G. Aeppli, and S. T. Bramwell, Brownian motion and quantum dynamics of magnetic monopoles in spin ice, Nat. Commun. **4**, 1535 (2013).

[44] C. Paulsen, S. R. Giblin, E. Lhotel, D. Prabhakaran, G. Balakrishnan, K. Matsuhira, and S. T. Bramwell, Experimental signature of the attractive Coulomb force between positive and negative magnetic monopoles in spin ice, Nat. Phys. **12**, 661 (2016).

[45] A. A. Lee, D. Vella, S. Perkin, and A. Goriely, Are room-temperature ionic liquids dilute electrolytes? J. Phys. Chem. Lett. **6**, 159 (2015).

[46] A. A. Lee, C. S. Perez-Martinez, A. M. Smith, and S. Perkin, Underscreening in concentrated electrolytes, Faraday Discuss. **199**, 239 (2017).

[47] W. Marshall and R. D. Lowde, Magnetic correlations and neutron scattering, Rep. Prog. Phys. **31**, 705 (1968).

[48] S. T. Bramwell, Harmonic phase in polar liquids and spin ice, Nat. Commun. **8**, 2088 (2017).

[49] J. F. Nye, *Physical Properties of Crystals* (Clarendon, Oxford, 1985).

[50] M. A. Subramanian, G. Aravamudan, and G. V. Subba Rao, Oxide pyrochlores—A review, Prog. Solid State Chem. **15**, 55 (1983).

[51] S. Rosenkranz, A. P. Ramirez, A. Hayashi, R. J. Cava, R. Siddharthan, and B. S. Shastry, Crystal-field interaction in the pyrochlore magnet $Ho_2Ti_2O_7$, J. Appl. Phys. **87**, 5914 (2000).

[52] A. Bertin, Y. Chapuis, P. Dalmas de Réotier, and A. Yaouanc, Crystal electric field in the $R_2Ti_2O_7$ pyrochlore compounds, J. Phys.: Condens. Matter **24**, 256003 (2012).

[53] Y. M. Jana, A. Sengupta, and D. Ghosh, Estimation of single ion anisotropy in pyrochlore $Dy_2Ti_2O_7$, a geometrically frustrated system, using crystal field theory, J. Magn. Magn. Mater. **248**, 7 (2002).

[54] J. G. Rau and M. J. P. Gingras, Magnitude of quantum effects in classical spin ices, Phys. Rev. B **92**, 144417 (2015).

[55] R. G. Melko and M. J. P. Gingras, Monte Carlo studies of the dipolar spin ice model, J. Phys.: Condens. Matter **16**, R1277 (2004).

[56] J. D. Bernal and R. H. Fowler, A theory of water and ionic solution, with particular reference to hydrogen and hydroxyl ions, J. Chem. Phys. **1**, 515 (1933).

[57] M. Twengström, L. Bovo, M. J. P. Gingras, S. T. Bramwell, and P. Henelius, Microscopic aspects of magnetic lattice demagnetizing factors, Phys. Rev. Mater. **1**, 044406 (2017).

[58] P. P. Ewald, Die berechnung optischer und elektrostatischer gitterpotentiale, Ann. Phys. (Leipzig) **369**, 253 (1921).

[59] R. G. Melko, B. C. den Hertog, and M. J. P. Gingras, Long-Range Order at Low Temperatures in Dipolar Spin Ice, Phys. Rev. Lett. **87**, 067203 (2001).

[60] M. Twengström, L. Bovo, O. A. Petrenko, B. Ouladdiaf, T. Fennell, P. Henelius, and S. T. Bramwell, Demagnetizing effects in the structure factor for diffuse neutron scattering (unpublished).

[61] M. Twengström, Spin ice and demagnetising theory, Ph.D. thesis, KTH Royal Institute of Technology, 2018.

[62] S. T. Bramwell, Generalized longitudinal susceptibility for magnetic monopoles in spin ice, Philos. Trans. R. Soc. A **370**, 5738 (2012).

[63] L. D. C. Jaubert, M. J. Harris, T. Fennell, R. G. Melko, S. T. Bramwell, and P. C. W. Holdsworth, Topological-Sector Fluctuations and Curie-Law Crossover in Spin Ice, Phys. Rev. X **3**, 011014 (2013).

[64] A. H. Morrish, *The Physical Principles of Magnetism* (Krieger, Malabar, 1980).

[65] L. Onsager, Electric moments of molecules in liquids, J. Am. Chem. Soc. **58**, 1486 (1936).

[66] L. Bovo, L. D. C. Jaubert, P. C. W. Holdsworth, and S. T. Bramwell, Crystal shape-dependent magnetic susceptibility and Curie law crossover in the spin ices $Dy_2Ti_2O_7$ and $Ho_2Ti_2O_7$, J. Phys.: Condens. Matter **25**, 386002 (2013).

[67] I. A. Ryzhkin, Frustration model of proton disorder in ice, Solid State Commun. **52**, 49 (1984).

[68] G. Sala, M. J. Gutmann, D. Prabhakaran, D. Pomaranski, C. Mitchelitis, J. B. Kycia, D. G. Porter, C. Castelnovo, and J. P. Goff, Vacancy defects and monopole dynamics in oxygen-deficient pyrochlores, Nat. Mater. **13**, 488 (2014).

[69] H. M. Revell, L. R. Yaraskavitch, J. D. Mason, K. A. Ross, H. M. L. Noad, H. A. Dabkowska, B. D. Gaulin, P. Henelius, and J. B. Kycia, Evidence of impurity and boundary effects on magnetic monopole dynamics in spin ice, Nat. Phys. **9**, 34 (2012).

[70] A. Ghasemi, A. Scheie, J. Kindervater, and S. M. Koohpayeh, The pyrochlore $Ho_2Ti_2O_7$: Synthesis, crystal growth, and stoichiometry, J. Cryst. Growth **500**, 38 (2018).

[71] L. Bovo, M. Twengström, O. A. Petrenko, T. Fennell, M. J. P. Gingras, S. T. Bramwell, and P. Henelius, Special temperatures in frustrated ferromagnets, Nat. Commun. **9**, 1999 (2018).

[72] I. Daruka and Z. Gulácsi, Correlation transitions in the Ising chain with competing short-range and long-range mirror interactions, Phys. Rev. E **58**, 5403 (1998).

[73] M. J. P. Gingras and P. A. McClarty, Quantum spin ice: A search for gapless quantum spin liquids in pyrochlore magnets, Rep. Prog. Phys. **77**, 056501 (2014).

[74] R. Moessner and S. L. Sondhi, Three-dimensional resonating-valence-bond liquids and their excitations, Phys. Rev. B **68**, 184512 (2003).

[75] M. Hermele, M. P. A. Fisher, and L. Balents, Pyrochlore photons: The $U(1)$ spin liquid in a $s = \frac{1}{2}$ three-dimensional frustrated magnet, Phys. Rev. B **69**, 064404 (2004).

[76] S. Onoda, Effective quantum pseudospin-1/2 model for Yb pyrochlore oxides, J. Phys.: Conf. Ser. **320**, 012065 (2011).

[77] A. H. Castro Neto, P. Pujol, and E. Fradkin, Ice: A strongly correlated proton system, Phys. Rev. B **74**, 024302 (2006).

[78] J. Gaudet, E. M. Smith, J. Dudemaine, J. Beare, C. R. C. Buhariwalla, N. P. Butch, M. B. Stone, A. I. Kolesnikov, G. Xu, D. R. Yahne, K. A. Ross, C. A. Marjerrison, J. D. Garrett, G. M. Luke, A. D. Bianchi, and B. D. Gaulin, Quantum Spin Ice Dynamics in the Dipole-Octupole Pyrochlore Magnet $Ce_2Zr_2O_7$, Phys. Rev. Lett. **122**, 187201 (2019).

[79] S. Petit, E. Lhotel, S. Guitteny, O. Florea, J. Robert, P. Bonville, I. Mirebeau, J. Ollivier, H. Mutka, E. Ressouche, C. Decorse, M. Ciomaga Hatnean, and G. Balakrishnan, Antiferroquadrupolar correlations in the quantum spin ice candidate $Pr_2Zr_2O_7$, Phys. Rev. B **94**, 165153 (2016).

[80] P. A. McClarty, O. Sikora, R. Moessner, K. Penc, F. Pollmann, and N. Shannon, Chain-based order and quantum spin liquids in dipolar spin ice, Phys. Rev. B **92**, 094418 (2015).

[81] C. Paulsen, S. R. Giblin, E. Lhotel, D. Prabhakaran, K. Matsuhira, G. Balakrishnan, and S. T. Bramwell, Nuclear spin

assisted quantum tunneling of magnetic monopoles in spin ice, Nat. Commun. **10**, 1509 (2019).

[82] O. Halpern and T. Holstein, On the passage of neutrons through ferromagnets, Phys. Rev. **59**, 960 (1941).

[83] R. M. Moon, T. Riste, and W. C. Koehler, Polarization analysis of thermal-neutron scattering, Phys. Rev. **181**, 920 (1969).

[84] D. J. Griffiths, Hyperfine splitting in the ground state of hydrogen, Am. J. Phys. **50**, 698 (1982).

[85] S. T. Banks and S. T. Bramwell, Magnetic frustration in the context of pseudo-dipolar ionic disorder, Europhys. Lett. **97**, 27005 (2012).

[86] O. Benton, Quantum origins of moment fragmentation in $Nd_2Zr_2O_7$, Phys. Rev. B **94**, 104430 (2016).

[87] H. Yan, R. Pohle, and N. Shannon, Half moons are pinch points with dispersion, Phys. Rev. B **98**, 140402(R) (2018).

[88] O. Benton, L. D. C. Jaubert, H. Yan, and N. Shannon, A spin-liquid with pinch-line singularities on the pyrochlore lattice, Nat. Commun. **7**, 11572 (2016).

[89] O. Benton, O. Sikora, and N. Shannon, Classical and quantum theories of proton disorder in hexagonal water ice, Phys. Rev. B **93**, 125143 (2016).

[90] P. A. McClarty, A. O'Brien, and F. Pollmann, Coulombic charge ice, Phys. Rev. B **89**, 195123 (2014).

[91] D. Slobinsky, L. Pili, and R.A. Borzi, The polarized monopole liquid: A Coulomb phase in a fluid of magnetic charges, Phys. Rev. B **100**, 020405 (2019).

[92] C. Gray, Field correlations in Coulomb gases, Ph.D. thesis, University College London, 2019.

[93] C. Gray, S. T. Bramwell, and P. C. W. Holdsworth, Electric field fluctuations in the two-dimensional Coulomb fluid, arXiv:1912.02243.